Journal Pre-proof

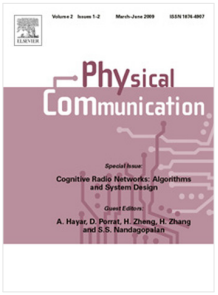

Framework for propagation modeling of IRS-assisted communication based on ray tracing

Mohammadreza Farashahi, Boon-Chong Seet, Xue Jun Li

PII: S1874-4907(24)00019-3
DOI: https://doi.org/10.1016/j.phycom.2024.102301
Reference: PHYCOM 102301

To appear in: *Physical Communication*

Received date : 17 May 2023
Revised date : 15 October 2023
Accepted date : 19 January 2024

Please cite this article as: M. Farashahi, B.-C. Seet and X.J. Li, Framework for propagation modeling of IRS-assisted communication based on ray tracing, *Physical Communication* (2024), doi: https://doi.org/10.1016/j.phycom.2024.102301.

Framework for Propagation Modeling of IRS-Assisted Communication based on Ray Tracing

Mohammadreza Farashahi[a], Boon-Chong Seet[a], Xue Jun Li[a]

[a]*Department of Electrical and Electronic Engineering, Auckland University of Technology, Auckland, 1010, New Zealand*

Abstract

Intelligent Reflecting Surface (IRS) is an emerging technology to improve the performance of wireless systems. As implementing IRS in a wireless network with complex indoor environments is a challenging task, how to perform a realistic simulation study of such a system becomes a necessary and important topic. This paper presents a framework for modeling wireless propagation channels for an IRS-based indoor wireless communication system. The framework adopts ray tracing as the base engine for calculating the power delay profile (PDP) of the transmission paths. Moreover, we propose an approximate method to speed up the simulation without compromising on the level of accuracy. The PDPs calculated by the framework are used to model a deterministic channel for a wireless communication system enhanced by a 20×20 IRS.

Keywords: Intelligent Reflecting Surface (IRS), Propagation Modeling, Ray Tracing, Wireless Communication, Optimization

1. Introduction

The flourishing of wireless systems is driven by the increasing number of subscribers and their demand for high data-rate, low latency multimedia services. [1–5]. To achieve this goal, several technologies, such as small cells [6], millimeter wave (mmWave) [7], and massive multiple-input multiple-output (MIMO) [8] have been introduced, most of which require increased hardware cost and energy consumption due to the expensive radio frequency (RF) components associated with higher operating frequency bands. This necessitates innovative, energy-friendly, and cost-effective approaches for next-generation wireless systems [9].

Recently, intelligent reflecting surfaces (IRSs) have been proposed as innovative conformal structures that are capable of reconfiguring the propagation environment [10, 11] while maintaining high spectral efficiency and energy efficiency. These structures have attracted substantial attention due to their low hardware footprint compared to facilities used in MIMO networks, making them extremely attractive to be deployed in large-scale urban structures in both indoor and outdoor environments. From a technical perspective, an IRS is a planar structure that is composed of periodic unit elements called meta-atoms, each of which can create a reflection phase delay when illuminated by electromagnetic (EM) waves. By controlling the reflection phase property of its unit elements, an IRS can alter the reflection pattern of the EM waves impinging on its surface. Active radio frequency (RF) lumped elements are embedded in each meta-atom to create a range of discrete or analog phase delays in the impinging EM waves [12–14].

In the literature, researchers have examined IRS structures from different aspects. For instance, in [15], a physics-based modeling of IRS structures was introduced, whereas in [16], the performance of IRSs was studied through field experiments. Several surveys in the literature delve into the implementation and applications of IRS [17–21]. In terms of the optimization of IRS elements, [22, 23] offer insights into optimizing the phase distribution of IRS elements in a variety of wireless communication systems, whereas [24, 25] studied approaches in channel state information (CSI) acquisition of IRS-assisted communication systems.

When considering propagation environments, particularly the complex ones, it is important to design a wireless system that ensures quality wireless links between transmitters (TXs) and receivers (RXs), which are least sensitive to the location of user equipment

Email address: reza.farashahi@aut.ac.nz (Mohammadreza Farashahi)

(UE) in the environment. As such, realistic simulation of target environments and deriving their propagation characteristics can be of great help to determine the strategic locations of the IRS. In this regard, several methods can be used for propagation modeling, namely finite-difference time-domain (FDTD) [26], finite element method (FEM) [27], method of moments (MoM) [28], and ray tracing (RT) method [29], all of which belong to the computational EM family. for large and complex environments, whether they are indoor or outdoor, ray tracing is considered one of the best candidates for propagation modeling as the method is exceptionally fast while being considerably accurate [30].

In this paper, a ray tracing-based framework for propagation modeling of an indoor environment for an IRS-assisted Single-Input Single-Output (SISO) wireless system is proposed. It is then used to model the channels between each TX and UE pair in scenarios where there is a lack of line-of-sight (LOS) link between them, but each has a direct sight to the IRS. Next, an approximate model of the original framework is proposed to significantly reduce the computation time. Both original (accurate) and approximate models are then used to generate deterministic channels for data transmission. Finally, the channels generated by both models are compared, and the approximate model's performance is further evaluated under changing UE position and IRS size.

The main contributions of this paper can be summarized as follows:

- Proposed a propagation modeling framework for indoor IRS-assisted communication based on ray tracing for the first time in literature to the best of our knowledge.
- Proposed a fast and accurate approximate model of our above framework, which vastly speeds up the simulation time while still achieving a similar accuracy level as the original model.
- Investigated and presented new insights on the impact of different UE positions and IRS sizes on the accuracy of such propagation models.

The remainder of the paper is organized as follows: Section 2 presents our proposed framework for the propagation modeling of IRS-assisted communication. Section 3 further presents an approximate model of our framework, and the results from both models are discussed in Section 4. Finally, the paper is concluded with some directions for future work in Section 5.

2. Proposed Framework

This section presents a framework for ray tracing-based propagation modeling of a SISO orthogonal frequency-division multiplexing (OFDM) system in an IRS-assisted indoor environment. Such a framework can also be utilized to model MIMO communication with some adaptation. This framework is subsequently used to model the wireless channel between each TX and RX in a three-dimensional (3D) indoor environment. In this framework, it is assumed that there is no LOS link between TX and UE, while LOS links exist between TX and IRS, and between UE and IRS. Furthermore, the maximum number of reflections for the rays sent from TX and subsequently received by UE is considered to be 2, as the effect of rays will become negligible after two reflections [18]. The IRS itself is composed of 20×20 elements, which are spaced at a distance of $\lambda/2$ with an operating frequency of 5.8 GHz.

In the first step, an indoor environment needs to be created. For this purpose, an existing office space model from MATLAB has been adopted to be incorporated into our framework as shown in Fig. 1. Note that other 3D environments can be created using software applications such as SketchUp and imported into our framework with different material types for surrounding walls and furniture. As seen in Fig. 1, the office has two rooms separated by a concrete partition blocking the LOS link between TX and UE. The TX is located in one room where it has direct sight to the IRS. The UE is located in the other room. Since ray tracing is used to model a deterministic channel between the TX and UE, the materials of objects and walls should be defined in order to accurately compute the path loss of each ray.

Subsequently, the power delay profile (PDP) of the channel between TX and UE will be calculated. Initially, the IRS is removed from the environment, and the PDP of the channel for TX-UE is calculated. At this stage, any rays intersecting with the IRS's location should be omitted from the PDP, as they will be incorporated in the subsequent step. Next, the PDP of the channel of TX-IRS-UE is calculated. In this step, the PDP between TX and each IRS element (a.k.a. unit cell) is calculated separately. As such, each cell is replaced by an isotropic antenna located at its center, and the PDP for the channels between IRS cell-TX, and between IRS cell-UE are calculated with ray tracing. An isotropic antenna in our case would mean that the IRS's unit cells are not sensitive to impinging rays' incident angle. The sensitivity pattern of a unit cell is dependent on the physical structure of the cell, and different structures can have different patterns. In the literature,

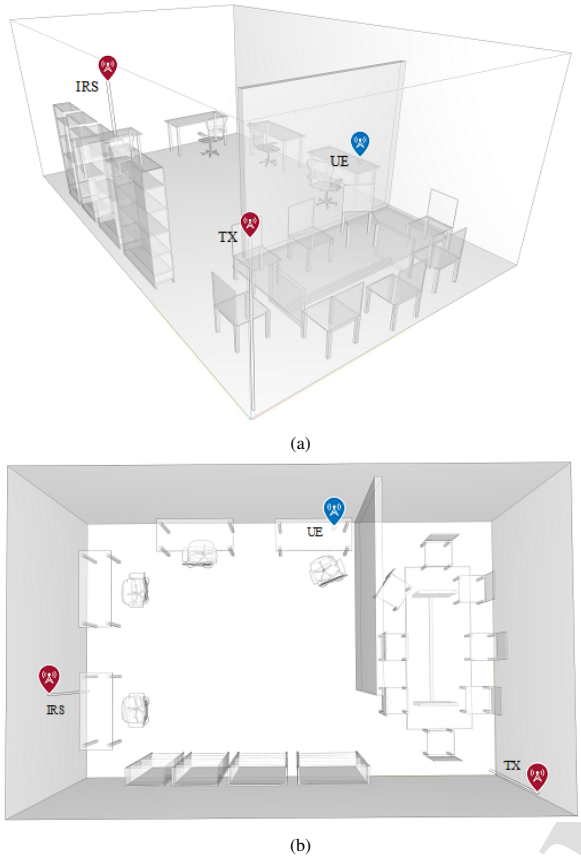

Figure 1: **(a)** Perspective view; and **(b)** Top view of the indoor environment that includes a TX, UE (RX), and IRS.

a variety of patterns have been investigated for an IRS unit cell [31]. Defining $d_{t,n}$ and $d_{r,n}$ as the distances between n^{th} IRS cell and TX, and between n^{th} IRS cell and RX, respectively, the total power of the transmitted rays bounced by the IRS and finally received at the UE can be calculated as [32]:

$$P_r^{TX-IRS-UE} = P_t G_t G_r \left(\frac{A}{4\pi}\right)^2 \left|\sum_{n=1}^{N} \frac{R_n e^{-j\Phi_n}}{d_{t,n} d_{r,n}}\right|^2, \quad (1)$$

$$\Phi_n = \frac{2\pi}{\lambda}(d_{t,n} + d_{r,n}) + \phi_n, \quad (2)$$

where P_t is the transmit power of TX, N is the number of cells, A is the surface area of the unit cell that captures and reflects each ray's transmit power [31], R_n and Φ_n are reflection loss and phase change for the n^{th} path, ϕ_n is phase shift of unit cells in the n^{th} cell, and G_t and G_r are antenna gain of TX, and UE, respectively. To enhance modeling precision, each ray from TX to the n^{th} IRS cell is broken into multiple rays traveling from the n^{th} cell to UE. For example, if the PDP for TX-IRS and IRS-UE channels for the n^{th} cell are modeled with $M_{t,n}$, and $M_{r,n}$ rays, respectively, there will be $M_{t,n} \times M_{r,n}$ rays for the n^{th} cell, totaling $M_{t,n} \times M_{r,n} \times N$ number of IRS-reflected rays as shown in Fig. 2. Fig. 2 (a) showcases a multitude of rays, each engaging with the individual unit cells of the IRS. Distinct clusters of rays, depicted with different color codes, represent groups of rays traversing analogous trajectories while interacting with diverse unit cells. In order to present the data in Fig. 2 (a) more clearly, data binning has been employed. The time span between 45 and 52 ns is segmented into 70 bins, and rays within the same bin are aggregated (see Fig. 2 (b)). Since each ray has magnitude and phase, the summation of the rays in the same bin would be the same as the summation of vectors. In the final step, rays bounced from the IRS are added to the non-IRS reflected rays.

In the next section, a faster framework based on approximating the channel calculation of an IRS-assisted indoor environment is introduced.

3. Proposed Approximate Model

To accurately model an indoor IRS-assisted communication, each ray traveling from TX to the n^{th} IRS cell and bouncing towards the UE needs to be traced and taken into account. However, the more accurate the model becomes, the more time it requires for the computation. For example, to model the PDP of an indoor 400-element IRS-assisted SISO system accurately with the ray tracing (RT) method, 400 RT realizations need to be performed between TX and IRS, and another 400 realizations between IRS and UE. Using a standard computer with a Core-i7 CPU and 32 GB of system memory, the run time to complete all simulations is 86.58 seconds. To improve the scalability of our proposed framework, an approximate method to model the same environment is further proposed.

In the approximate model, only 3 RT realizations are needed to be performed between TX and UE (rays interacting with IRS are to be removed), TX and IRS's center, and UE and IRS's center. Initially, all rays between TX and IRS's center; UE and IRS's center are found, and the reflection point and loss of each ray are collected. Next, Euclidean distances between TX and IRS unit cells; UE and IRS unit cells; TX and reflection points; UE and reflection points; and reflection points and IRS unit cells are computed. With the available distances, all possible TX-IRS-UE paths can be calculated. For further illustration, Fig. 3 depicts a simplified two-dimensional (2D) environment with a 3-cell IRS where

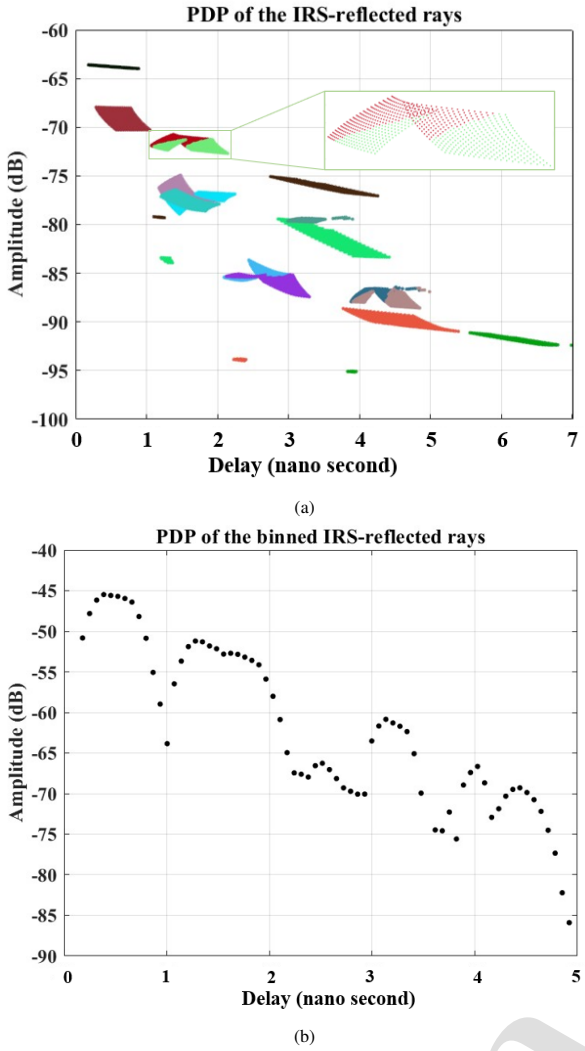

Figure 2: Power Delay Profile of IRS-reflected rays calculated with accurate model **(a)** Without data binning; and **(b)** With data binning using 70 bins in time axis. The sub-figure **(a)** shows clusters of rays grouped by different colors. Each cluster contains 400 rays reflected from the IRS surface, each from a different unit cell.

the black and green lines represent the TX-IRS-UE, and TX-UE ray paths, respectively. In the final step, the path loss and phase shift of each ray can be calculated with its corresponding propagation distance, the phase shift of each unit cell, and reflection loss. For rays that do not interact with IRS, their propagation loss and phase are calculated by:

$$|P_r|_{dB} = G_{t,dB} + G_{r,dB} - FSPL(d_t) - L_{reff} \quad (3)$$

$$\angle P_r = e^{j\frac{2\pi}{\lambda}d_t} \quad (4)$$

where $FSPL(\cdot)$ is propagation loss in free space, d_t is the total propagation distance of each ray, and L_{ref} is the reflection coefficient of the material of the object that reflects the ray (e.g., concrete, wood, etc.) On the other hand, for rays interacting with IRS, equations (1) and (2) are used to calculate the rays' amplitude and phase. However, the reflection loss of the environment and IRS should also be taken into account. The reflection coefficient of each unit cell is highly dependent on its structural parameters, such as the number and material of dielectric layers, conductor layers' pattern, and lumped elements used. The variation of reflection loss is expected to be between approximately 0.1-3 dB based on the measured values given in [13, 14, 33]. While the parameter can be modified in the model for specific unit cell structures, we have considered the worst-case scenario for the IRS reflection loss of 3 dB in all calculations in this paper.

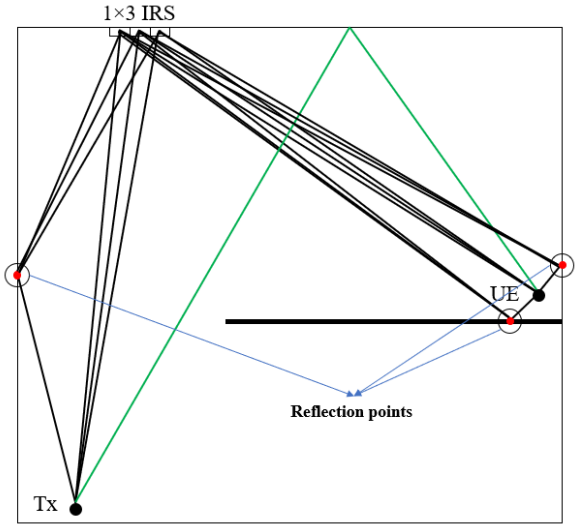

Figure 3: 2D simplified environment of the office room in Fig. 1.

Fig. 4 depicts the procedural steps of both accurate and approximate models for calculating the channels between TX-UE with IRS assistance. It is notable that each blue block represents an RT realization calculating rays between different points in the environment. The primary computational overhead stems from these blocks. Minimizing the number of executions of these blocks would result in a notable reduction in overall processing time. For the given environment, the accurate model requires a total of 801 RT realizations, while the approximate model requires only 3 realizations, significantly reducing the total run time by 99.6% from 86.58 to 0.35 seconds. Fig. 5 shows the amplitude of the PDP

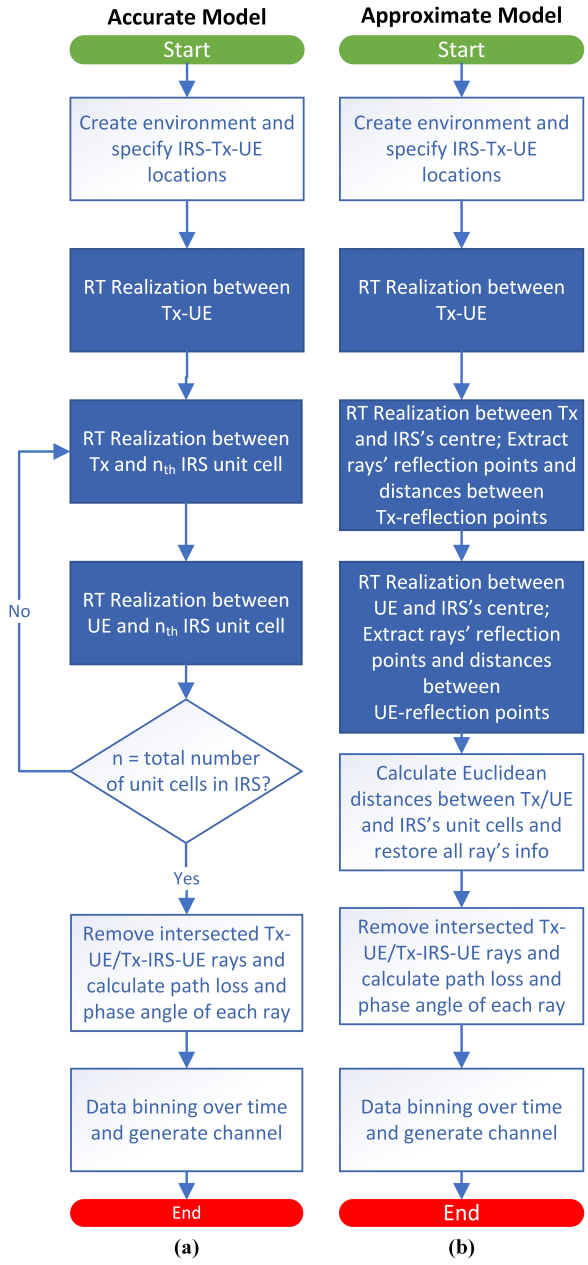

Figure 4: Frameworks for **(a)** accurate; and **(b)** approximate modeling of deterministic channels in IRS-assisted indoor environments.

of TX-IRS-UE rays calculated by the proposed approximate approach. It illustrates that the achieved accuracy is similar to that of the accurate model. Fig. 6 showcases a direct comparison of the total PDPs generated by the two different models. Notably, the PDP curves show a clear similarity, highlighting the effectiveness of

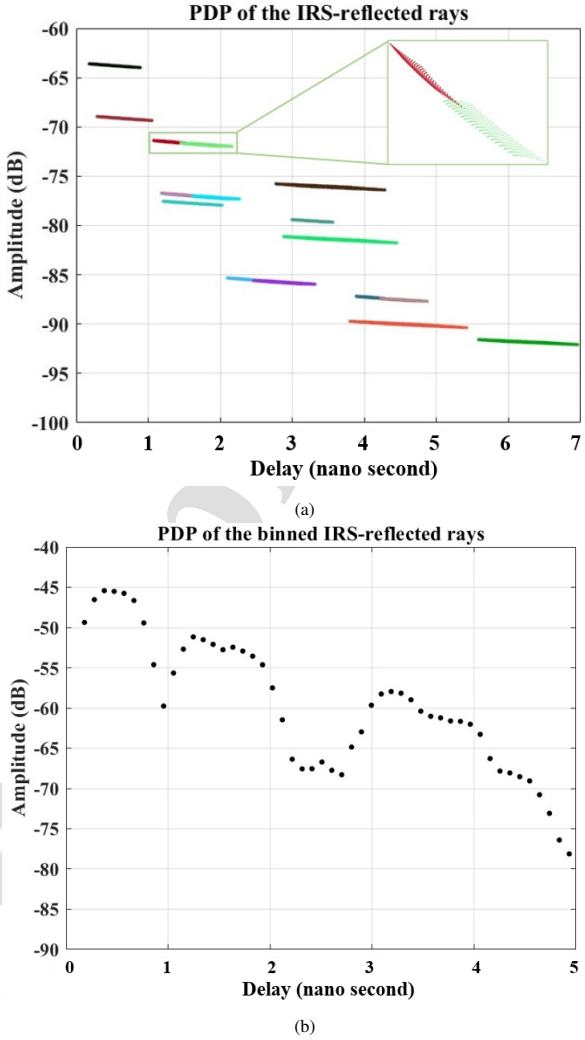

Figure 5: Power Delay Profile of IRS-reflected rays calculated with approximate model **(a)** Without data binning; and **(b)** With data binning using 70 bins in time axis.

the approximate model in capturing the detailed timing patterns of wireless channel behavior.

4. Results and Discussion

In this section, two deterministic channel models are developed based on the computed PDPs, through which data are transmitted from TX to UE. The system setup is shown in Fig. 7.

At the transmitter, data is encoded using a 1/2 Low-Density Parity-Check (LDPC) encoder. The encoded data is subsequently mapped onto Quadrature Amplitude Modulation (QAM) symbols via a 16-QAM mod-

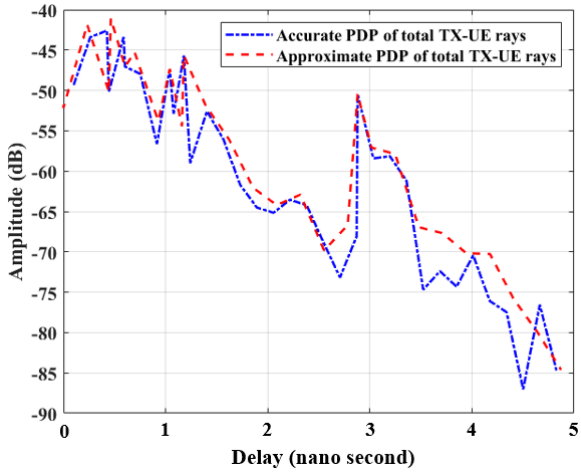

Figure 6: Comparison between the total PDPs calculated by accurate and approximate RT models.

ulator block. These modulated symbols are further processed through an Orthogonal Frequency Division Multiplexing (OFDM) block. This block segments the data into 214 sub-carriers, consisting of 25 pilots and 17 guard bands. The resultant signal is then added with Gaussian white noise and transmitted through a channel generated by both accurate and approximate ray-tracing models.

Upon reception, the received data is processed through a reverse OFDM block. Leveraging OFDM pilots, this block estimates the channel's characteristics. QAM symbols are then extracted based on the equalized channel and passed to subsequent stages, including QAM demodulation and channel decoding blocks. Throughout this process, several key parameters are evaluated, including estimated amplitude and gain of the channel and Bit Error Rate (BER).

Fig. 8 illustrates the channel gains between TX and UE calculated with accurate and approximate PDPs. Transmission is done in the presence of an IRS whose elements' phase shift is set to zero, and the locations of the TX, UE, and IRS are assigned as shown in Fig. 1. Fig. 9 (a) and (b) depict the IRS phase shifts optimized for minimal BER calculated by the approximate and accurate models, respectively. The optimization process employs a single objective Genetic Algorithm (GA), where the solution space comprises a 400-element array, with each element spanning between 0 and 360 degrees. The GA operates with a population size of 200 and terminates when the derivative between two successive solutions (BERs) reaches a threshold of 1e-5. Fig. 9 (c) depicts the difference between the phase distributions

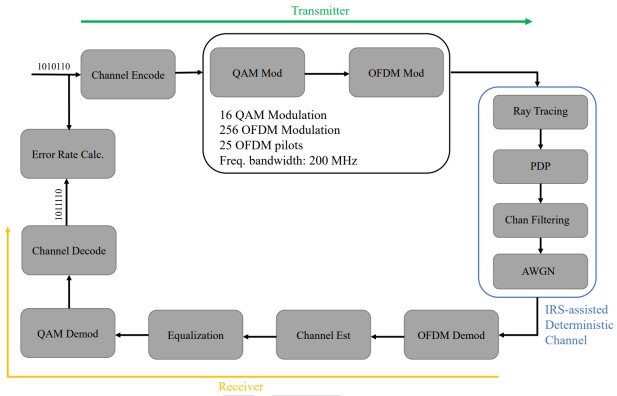

Figure 7: System setup for data transmission.

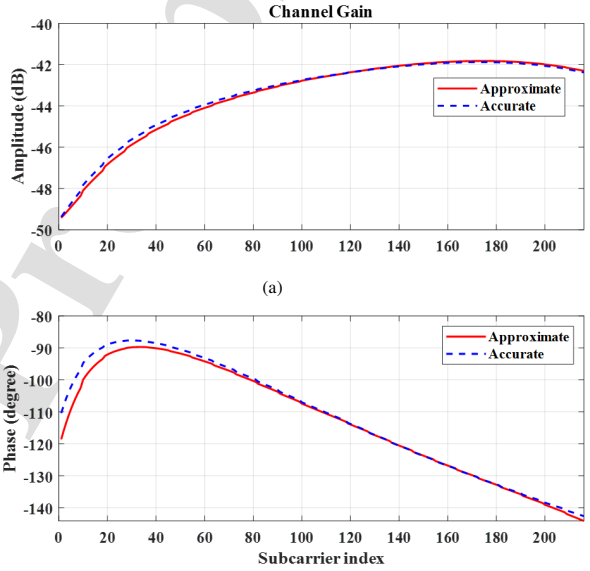

Figure 8: **(a)** Amplitude; and **(b)** Phase of the channel gains derived from accurate and approximate PDPs.

of both models. It can be seen that the phase error for each unit cell ranges between $-8°$ and $6°$. To verify the models statistically, they are further evaluated under 100 random TX and UE locations. For each of the 100 locations, the direct path between TX and UE is blocked, while both have direct sight to the IRS. Fig. 10 shows the probability density function (PDF) of the phase error between accurate and approximate models for each IRS unit cell. The results show that the mean phase error value is close to 0, while the phase error range mostly falls between $\pm 5°$.

Fig. 11 illustrates the phase error PDF for three IRS

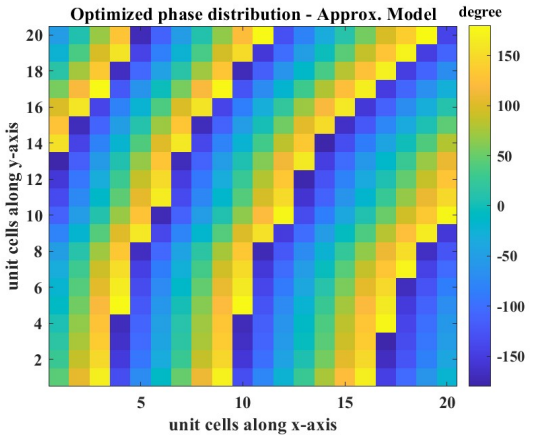

(a)

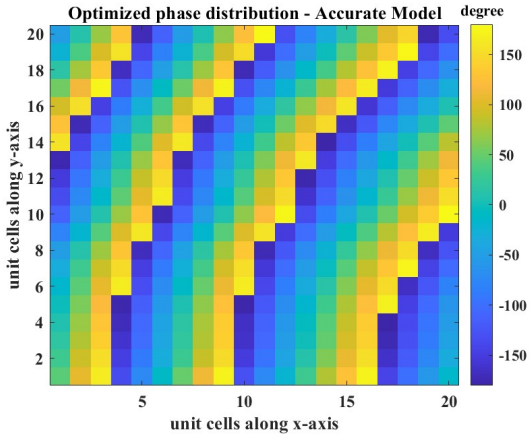

(b)

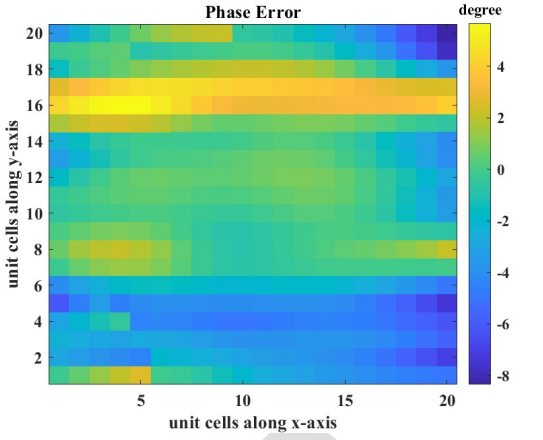

(c)

Figure 9: Optimized IRS phase distribution generated by: **(a)** Approximate model; and **(b)** Accurate model. The sub-figure **(c)** shows the difference between **(a)** and **(b)**.

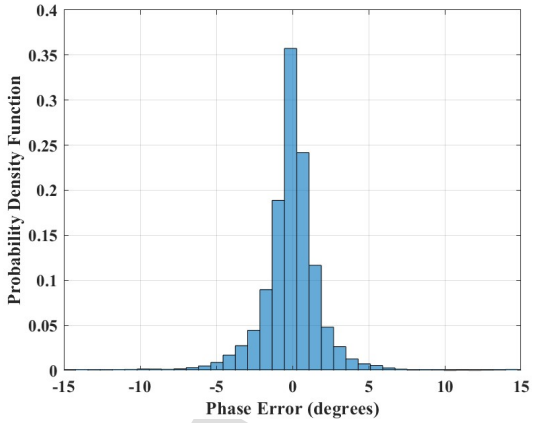

Figure 10: PDF of unitcell's phase error between accurate and approximate models.

sizes: 5×5, 20×20, and 40×40. Since the distance between unit cells is maintained at $\lambda/2$, an increase in the number of IRS unit cells translates to a physically expansive IRS structure. Expectedly, the phase error range increases with the IRS size, which may be reduced by grouping the unit cells. Fig. 12 evaluates the BER obtained by both models as a function of E_b/N_0 where a 20×20 IRS is deployed. The results show that the BER values are acceptable under a moderate to high E_b/N_0, and the performances of both models are strikingly similar, underlining the accuracy of the approximate approach even for a considerably large IRS structure.

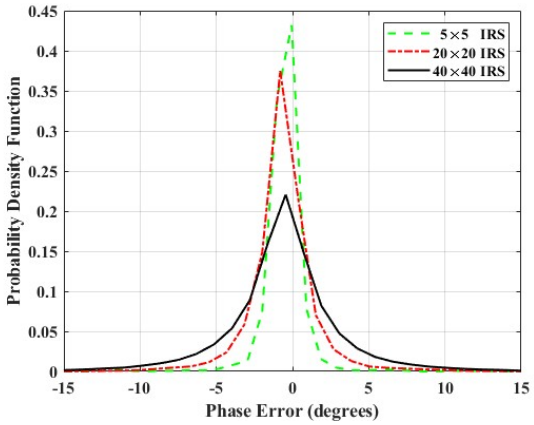

Figure 11: PDF of unitcell's phase error for 5×5, 20×20, and 40×40 IRS structures.

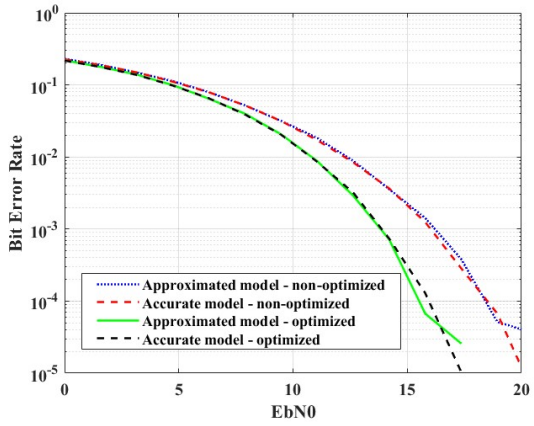

Figure 12: BER of IRS-assisted communication calculated with approximate and accurate PDPs for different values of E_b/N_0.

5. Conclusion and Future Works

This paper proposes a framework for propagation modeling of IRS-assisted communication based on ray tracing for indoor environments. The framework can serve as a tool to investigate the propagation characteristics of a specific environment based on the location of the IRS and communication devices for estimating the performance of an IRS-assisted wireless system. The framework has been further simplified through approximations in order to reduce the computation time. The results have demonstrated that the approximate model can perform as accurately as the non-approximate model while reducing the run time by 99.6% for a considerably large IRS structure with 400 elements. Future work may focus on investigating the scalability of the framework to enable the modeling of more complex propagation environments with multiple IRSs and MIMO devices. In addition, work may be extended to outdoor environments for estimating the performance of IRSs in future 6G and mmWave systems in different scenarios.

References

[1] A. Al-Fuqaha, M. Guizani, M. Mohammadi, M. Aledhari, M. Ayyash, Internet of things: A survey on enabling technologies, protocols, and applications, IEEE Communications Surveys & Tutorials 17 (4) (2015) 2347–2376.

[2] K. David, H. Berndt, 6G vision and requirements: Is there any need for beyond 5G?, IEEE Vehicular Technology Magazine 13 (3) (2018) 72–80.

[3] W. Saad, M. Bennis, M. Chen, A vision of 6G wireless systems: Applications, trends, technologies, and open research problems, IEEE Network 34 (3) (2019) 134–142.

[4] W. Zhou, J. Xia, F. Zhou, L. Fan, X. Lei, A. Nallanathan, G. K. Karagiannidis, Profit maximization for cache-enabled vehicular mobile edge computing networks, IEEE Transactions on Vehicular Technology (2023).

[5] X. Zheng, F. Zhu, J. Xia, C. Gao, T. Cui, S. Lai, Intelligent computing for wpt–mec-aided multi-source data stream, EURASIP Journal on Advances in Signal Processing 2023 (1) (2023) 1–17.

[6] J. Wang, W. Guan, Y. Huang, R. Schober, X. You, Distributed optimization of hierarchical small cell networks: A GNEP framework, IEEE Journal on Selected Areas in Communications 35 (2) (2017) 249–264.

[7] M. Xiao, S. Mumtaz, Y. Huang, L. Dai, Y. Li, M. Matthaiou, G. K. Karagiannidis, E. Björnson, K. Yang, I. Chih-Lin, Millimeter wave communications for future mobile networks, IEEE Journal on Selected Areas in Communications 35 (9) (2017) 1909–1935.

[8] V. Jungnickel, K. Manolakis, W. Zirwas, B. Panzner, V. Braun, M. Lossow, M. Sternad, R. Apelfröjd, T. Svensson, The role of small cells, coordinated multipoint, and massive MIMO in 5G, IEEE Communications Magazine 52 (5) (2014) 44–51.

[9] S. N. Sur, R. Bera, Intelligent reflecting surface assisted mimo communication system: A review, Physical Communication 47 (2021) 101386.

[10] W. Tang, M. Z. Chen, X. Chen, J. Y. Dai, Y. Han, M. Di Renzo, Y. Zeng, S. Jin, Q. Cheng, T. J. Cui, Wireless communications with reconfigurable intelligent surface: Path loss modeling and experimental measurement, IEEE Transactions on Wireless Communications 20 (1) (2020) 421–439, publisher: IEEE.

[11] S. F. Zamanian, S. M. Razavizadeh, 3d beamforming in intelligent reflecting surface (irs)-assisted multi-user cognitive radio networks, Physical Communication 56 (2023) 101951.

[12] F. Liu, O. Tsilipakos, A. Pitilakis, A. C. Tasolamprou, M. S. Mirmoosa, N. V. Kantartzis, D.-H. Kwon, J. Georgiou, K. Kossifos, M. A. Antoniades, Intelligent metasurfaces with continuously tunable local surface impedance for multiple reconfigurable functions, Physical Review Applied 11 (4) (2019) 044024.

[13] L. Dai, B. Wang, M. Wang, X. Yang, J. Tan, S. Bi, S. Xu, F. Yang, Z. Chen, M. Di Renzo, others, Reconfigurable intelligent surface-based wireless communications: Antenna design, prototyping, and experimental results, IEEE Access 8 (2020) 45913–45923, publisher: IEEE.

[14] Q. Ma, G. D. Bai, H. B. Jing, C. Yang, L. Li, T. J. Cui, Smart metasurface with self-adaptively reprogrammable functions, Light: Science & Applications 8 (1) (2019) 98, publisher: Nature Publishing Group UK London.

[15] M. Najafi, V. Jamali, R. Schober, H. V. Poor, Physics-based modeling and scalable optimization of large intelligent reflecting surfaces, IEEE Transactions on Communications 69 (4) (2020) 2673–2691, publisher: IEEE.

[16] W. Tang, M. Z. Chen, J. Y. Dai, Y. Zeng, X. Zhao, S. Jin, Q. Cheng, T. J. Cui, Wireless communications with programmable metasurface: New paradigms, opportunities, and challenges on transceiver design, IEEE Wireless Communications 27 (2) (2020) 180–187.

[17] K. O. Odeyemi, P. A. Owolawi, O. O. Olakanmi, Reconfigurable intelligent surface assisted mobile network with randomly moving user over fisher-snedecor fading channel, Physical Communication 43 (2020) 101186.

[18] Q. Wu, S. Zhang, B. Zheng, C. You, R. Zhang, Intelligent reflecting surface-aided wireless communications: A tutorial, IEEE Transactions on Communications 69 (5) (2021) 3313–3351, publisher: IEEE.

[19] Q. Wu, R. Zhang, Towards smart and reconfigurable environment: Intelligent reflecting surface aided wireless network,

IEEE Communications Magazine 58 (1) (2019) 106–112, publisher: IEEE.

[20] M. A. ElMossallamy, H. Zhang, L. Song, K. G. Seddik, Z. Han, G. Y. Li, Reconfigurable intelligent surfaces for wireless communications: Principles, challenges, and opportunities, IEEE Transactions on Cognitive Communications and Networking 6 (3) (2020) 990–1002, publisher: IEEE.

[21] M. Di Renzo, A. Zappone, M. Debbah, M.-S. Alouini, C. Yuen, J. De Rosny, S. Tretyakov, Smart radio environments empowered by reconfigurable intelligent surfaces: How it works, state of research, and the road ahead, IEEE Journal on Selected Areas in Communications 38 (11) (2020) 2450–2525, publisher: IEEE.

[22] C. Huang, A. Zappone, G. C. Alexandropoulos, M. Debbah, C. Yuen, Reconfigurable intelligent surfaces for energy efficiency in wireless communication, IEEE Transactions on Wireless Communications 18 (8) (2019) 4157–4170, publisher: IEEE.

[23] Q. Wu, R. Zhang, Joint active and passive beamforming optimization for intelligent reflecting surface assisted SWIPT under QoS constraints, IEEE Journal on Selected Areas in Communications 38 (8) (2020) 1735–1748, publisher: IEEE.

[24] P. Wang, J. Fang, H. Duan, H. Li, Compressed channel estimation for intelligent reflecting surface-assisted millimeter wave systems, IEEE Signal Processing Letters 27 (2020) 905–909, publisher: IEEE.

[25] L. Wei, C. Huang, G. C. Alexandropoulos, C. Yuen, Z. Zhang, M. Debbah, Channel estimation for RIS-empowered multi-user MISO wireless communications, IEEE Transactions on Communications 69 (6) (2021) 4144–4157, publisher: IEEE.

[26] S. C. Hagness, A. Taflove, Computational Electrodynamics: The Finite-Difference Time-Domain Method, Norwood, MA: Artech House (2000).

[27] J.-M. Jin, The finite element method in electromagnetics, John Wiley & Sons (2015).

[28] R. F. Harrington, J. L. Harrington, Field computation by moment methods, Oxford University Press, Inc. (1996).

[29] C.-F. Yang, B.-C. Wu, C.-J. Ko, A ray-tracing method for modeling indoor wave propagation and penetration, IEEE Transactions on Antennas and Propagation 46 (6) (1998) 907–919.

[30] Z. Yun, M. F. Iskander, Ray tracing for radio propagation modeling: Principles and applications, IEEE access 3 (2015) 1089–1100.

[31] W. Tang, X. Chen, M. Z. Chen, J. Y. Dai, Y. Han, M. Di Renzo, S. Jin, Q. Cheng, T. J. Cui, Path loss modeling and measurements for reconfigurable intelligent surfaces in the millimeter-wave frequency band, IEEE Transactions on Communications 70 (9) (2022) 6259–6276.

[32] O. Özdogan, E. Bjornson, E. G. Larsson, Intelligent reflecting surfaces: Physics, propagation, and pathloss modeling, IEEE Wireless Communications Letters 9 (5) (2019) 581–585, publisher: IEEE.

[33] H. Zhao, Y. Shuang, M. Wei, T. J. Cui, P. d. Hougne, L. Li, Metasurface-assisted massive backscatter wireless communication with commodity Wi-Fi signals, Nature Communications 11 (1) (2020) 3926, publisher: Nature Publishing Group UK London.

Mohammadreza Farashahi attained his Bachelor of Science degree in Electrical Engineering from Shahid Bahonar University of Kerman, Kerman, Iran, in 2014. He pursued a master's degree in Telecommunication Engineering from Shiraz University of Technology, Shiraz, Iran, culminating in his graduation in 2018. He is currently a Ph.D. at Auckland University of Technology, Auckland, New Zealand.

The primary focus of his research lies in the exploration of futuristic wireless communication systems, ranging from propagation modelling and channel estimation of IRS-assisted communication to designing metasurface structures at the physical level.

Mohammadreza Farashahi: Writing- Original draft preparation, Conceptualization, Methodology, Software, Visualization. **Boon-Chong Seet:** Supervision, Writing-Reviewing and Editing. **Xuejun Li:** Supervision, Writing-Reviewing and Editing

Declaration of interests

☒ The authors declare that they have no known competing financial interests or personal relationships that could have appeared to influence the work reported in this paper.

☐ The authors declare the following financial interests/personal relationships which may be considered as potential competing interests: